Chemical and Electrochemical Alkali Cations Intercalation/Release in an Ionic Hydrogen Bonded Network

Geoffrey Gerer, Frédéric Mélin, Petra Hellwig, Mir Wais Hosseini, Sylvie Ferlay

Chemical and electrochemical alkali cations intercalation/release in an ionic hydrogen bonded network

Geoffrey Gerer,[a,b] Frédéric Melin,[b] Petra Hellwig,[b] Mir Wais Hosseini[a*] and Sylvie Ferlay[a*]*

[a] Molecular Tectonics Laboratory, University of Strasbourg, UMR UDS-CNRS 7140, Institut le Bel, 4, rue Blaise Pascal, F-67000 Strasbourg, France
ferlay@unistra.fr, hosseini@unistra.fr

[b] Laboratoire de Bioélectrochimie et Spectroscopie, University of Strasbourg, UMR UDS-CNRS 7140, Institut le Bel, 4, rue Blaise Pascal, F-67000 Strasbourg, France
hellwig@unistra.fr

ABSTRACT

The chemical oxidation of a hydrogen bonded network, formed upon combination of a hydrogen bond donor dication (**1**$^{2+}$, a dicationic bis-amidinium organic moieties bearing four propyl chains) with $[Fe^{III/II}(CN)_6]^{3-/4-}$ anions has been studied using vibrational spectroscopies. The post synthetic oxidation of the microcrystalline powder of X_2**1**$_3$-$[Fe^{II}(CN)_6]_2$ (X = Na, K and Cs) by $S_2O_8^{2-}$ into **1**$_3$-$[Fe^{III}(CN)_6]_2$ appeared to be partial for X = K^+ and Cs^+ and total for Na_2**1**$_3$-$[Fe^{II}(CN)_6]_2$. It corresponds to a two-step process involving a second order reaction. The reaction time appears to be dependent on the nature of the alkali cation and is faster for X = Na^+. The integrity of the hydrogen bonded network, after oxidation, was also confirmed by XRPD. The flexible nature of

the hydrogen bonded network allows alkali cation motions within the network during the oxidation process. In addition, the investigation of the electrochemical behavior evidenced an amorphous deposition on a gold electrode immersed into a solution containing ($\mathbf{1}^{2+}$ and $[Fe^{III}(CN)_6]^{3-}$) after 100 cycles. This is the first evidence of an electrochemical ion intercalation for a molecular hydrogen bonded network.

Introduction

Electrochemical energy storage materials exhibiting high energy density and good cycling stability have attracted significant attention because of an increasing demand in the field of consumer electronics, or, for example, electric vehicles.[1,2] Within these lines, molecular compounds are studied with growing interest including highly ordered and robust molecular compounds such as coordination polymers[3,4,5] or hydrogen bonded networks.[6,7,8,9] In the latter case, their high degree of flexibility allows the fine tuning of their properties.

These extended periodic materials, able to store ions or to conduct protons, are thus of crucial interest for the development of new materials for energy storage and batteries. Compounds such as oxides, sulfides and polyanionic intercalated compounds,[10] were studied in order to enhance the performance of lithium-ion or sodium-ion batteries (LIBs or SIBs).[11] Coordination polymers have been exploited in recent years for energy storage materials such as lithium ion batteries, though they present an intrinsic low electronic conductivity.[12,13,14,15] For example, cyano bridged coordination polymers, Prussian Blue analogs (involving cyanometallates), with intercalated alkali and alkaline earth cations, have been reported as a new class of anode materials for ion batteries.[16,17,18,19]

Another application involving the use of molecular compounds for energy storage are polymer electrolyte membrane fuel cells (PEMFCs). These systems require proton-conducting pathways, such as hydrogen-bonded assemblies, to establish proton transport. In order to increase the transport of ions in materials dedicated to energy storage, several approaches have been reported like, the use of ionic liquid membranes[20] or hydrogels,[21] for example. Highly ordered materials, however, have been scarcely considered for such applications. MOFs and related materials are promising candidates for membranes in PEMFCs.[12,15,22] Dealing with H-bonded networks, they are mainly based on anionic recognition centers bearing chemical groups such as sulfonates, phosphonates, carboxylates that, under certain conditions, can take part in proton conduction.

For this reason, we intend to explore the redox and electrochemical properties of crystalline hydrogen bonded networks involving cyanometallates. This type of solid-state electrochemical reactions involving ion intercalation, are interesting when they are not confined to the surface of the compounds but express bulk behavior. The electrochemical behavior of microparticles of bimetallic octacyanometallates has been reported.[23] In addition, the use of bimetallic hexacyanoferrate,[24] octacyanotungstate[25] or octacyanomolybdate[26] bridged coordination polymers, with a Li intercalator, have been used as working electrode in an electrochemical experiment.

Using hydrogen bonded networks for the formation of electrochemically driven materials is of interest, however, it has not been reported so far. There are some examples involving coordination complexes.[27] In this work, we have used a network based on $[Fe^{III/II}(CN)_6]^{3-/4-}$ species, chosen for their electrochemical properties and the nanopatterned structures they may offer. The use of hexacyanoferrate(II) or (III) in hydrogen bonded networks has been already documented. The formation of robust networks based on the recognition between cations and anions, through charge

assisted hydrogen bonds (CAHB),[28] leads to H-bonded networks that may be candidates of choice for applications in the field of proton conduction, sensing, separation or guest exchange.[29,30,31,32] Hexacyanoferrate(II) building blocks have been assembled with cationic bisamidinium ($\mathbf{1}^{2+}$, Figure 1) N Hydrogen bond donors[33] designed for the recognition of hydrogen bond acceptors like cyanometallate, leading to robust hydrogen bonded networks.[34,35,36,37]

In this work, we have studied the post-synthetic chemical oxidation of a highly flexible organized hydrogen bonded networks for the preparation of both crystals and films, that may be electrochemically driven in the solid state, for the intercalation/release of alkali cations. For this purpose, the 2D networks $X_2\mathbf{1}_3$-$[Fe^{II}(CN)_6]_2$ (where X = Na, K or Cs, and $\mathbf{1}^{2+}$ is tris(2,2'-Benzene-1,4-diylbis(5,5-di-n-propyl-3,4,5,6-tetrahydropyrimidin-1-ium), were prepared and their oxidation was studied using *in-situ* IR/Raman investigations. The redox process was also studied by cyclic voltammetry experiments.

Experimental Section

Synthesis of compounds and crystals

The synthesis, complete characterization and solid-state structures of $X_2\mathbf{1}_3$-$[Fe^{II}(CN)_6]_2$ (X = K, Na or Cs CCDC refcode: PURMAR, PURLOE and PURLIY respectively)[39] and $\mathbf{1}_3$-$[Fe^{III}(CN)_6]_2$[38] (CCDC ref codes: PEQNAB) have been reported before. For the presented work, all compounds have been synthetized using the already reported procedure, and used as single crystals; their purity has been checked using IR measurements (figure S1, Supporting Information), XRPD (figure S2, Supporting Information) and also elemental analysis as shown in SI.

All experiments have been performed in air and at RT on freshly prepared single crystals or polycrystalline samples.

Instrumentation

Infrared Spectroscopy

Infrared spectra were obtained with a Vertex 70 FTIR spectrometer (Bruker, Karlsruhe, Germany) equipped with a ZnSe/Si ATR crystal from Harrick, USA. A KBr beamsplitter and a MCT detector were used. For each spectrum, 256 scans at a resolution of 4 cm^{-1} were recorded. A baseline correction was applied with OPUS software provided by Bruker.

Raman Spectroscopy

Raman spectra were measured with a Raman Renishaw Invia microscope operating at 514 nm. Each spectrum was acquired with 10 s irradiation time and 10% of the maximum laser power (25 mW).

SEM microscopy

The SEM images were recorded using a FEI Quanta 250 FEG microscope in high vacuum, with a spot size of 3 nm and acceleration voltage of 20 kV.

Electrochemical measurements

Cyclic voltammetry experiments were carried out at room temperature (20 ± 2 °C) in a standard three-electrode cell connected to a Princeton Applied Research VERSASTAT 4 potentiostat. An AgCl / Ag 3M NaCl was used as reference electrode and a platinum wire as counter electrode. Working electrodes were either a 3 mm diameter gold disk or a Si/Au substrate.

Chemical Oxidation conditions for IR measurements

About 5 mg of a polycrystalline sample of $X_2\mathbf{1}_3$-$[Fe^{II}(CN)_6]_2$ (X = Na, K and Cs) were deposited on a Si-coated ZnSe ATR crystal and equilibrated with the solvent mixture (10% Water/90% Methanol). An oxidant ($K_2S_2O_8$) solution (8.3 10^{-4} $molL^{-1}$) was then pumped through at a constant flow rate of 0.2 $mLmin^{-1}$. Spectra were recorded every 2 or 3 minutes.

Chemical Oxidation conditions for Raman measurements

2 mg of polycrystalline sample were immersed in 10 ml of the solvent mixture (10% Water/90% Methanol) containing 14 eq of $K_2S_2O_8$. The laser of the Raman microscope was focused on a crystal of 5µmx2µmx1µm approximate size. Spectra were recorded every 15 minutes.

Electrode-Modification Method: adsorption of crystals

$Na_2\mathbf{1}_3$-$[Fe^{II}(CN)_6]_2$ or $\mathbf{1}_3$-$[Fe^{III}(CN)_6]_2$ was transferred to the surface of a Si/Au substrate by immersion into a 1/1 H_2O/MeOH mixture containing either ($Na_4[Fe^{II}(CN)_6]$ + **1**-2Cl in 2/3 ratio) or into a 1/1 H_2O/MeOH mixture of ($K_3[Fe^{III}(CN)_6]$ + **1**-2Cl in 2/3 ratio) respectively.

Results and discussion

A preliminarily study evidenced, for these systems, the formation of hydrogen bonded networks when combining the hydrogen bond donor cation $\mathbf{1}^{2+}$ (tris(2,2'-Benzene-1,4-diylbis(5,5-di-n-propyl-3,4,5,6-tetrahydropyrimidin-1-ium, figure 1) with the $K_3Fe^{III}(CN)_6$, leading to the formation of a neutral hydrogen bonded network of formula $\mathbf{1}_3$-$[Fe^{III}(CN)_6]$[38] presenting a honey-comb like structure where each cation is surrounded by two $[Fe^{III}(CN)_6]^{3-}$ anions and each anion is surrounded by two $\mathbf{1}^{2+}$ cations. The combination of $X_4Fe^{II}(CN)_6$ with $\mathbf{1}^{2+}$, leads to a series of similar honeycomb-like compounds of formula $X_2\mathbf{1}_3$-$[Fe^{II}(CN)_6]_2$ (X = Na, K, Rb or Cs) (figure

1).[39] This series is isostructural with $\mathbf{1}_3$-$[Fe^{III}(CN)_6]_2$. Within this family, the compound presenting the closest metrics to $\mathbf{1}_3$-$[Fe^{III}(CN)_6]_2$ is $Cs_2\mathbf{1}_3$-$[Fe^{II}(CN)_6]$ and for this reason, we showed that it was possible to obtained the mixed valence system of composition $((Cs_2\mathbf{1}_3\text{-}[Fe^{II}CN)_6]_2)_{0.83}$-$(\mathbf{1}_3\text{-}[Fe^{III}(CN)_6]_2)_{0.15}$)).[39]

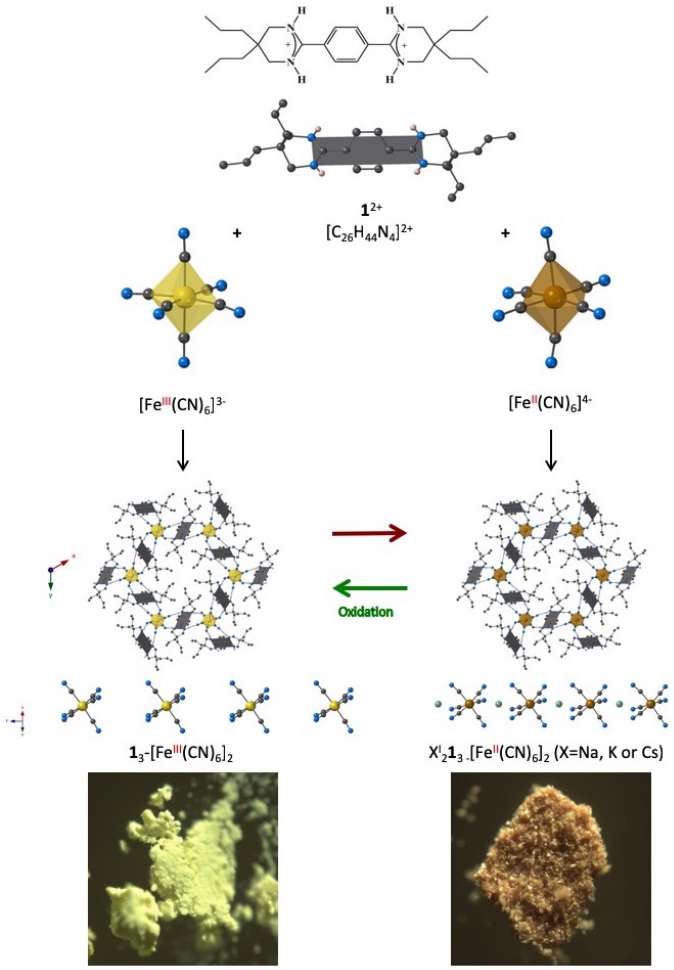

Figure 1. Formation of the hydrogen bonded networks $\mathbf{1}_3$-$[Fe^{III}(CN)_6]_2$ and $X_2\mathbf{1}_3$-$[Fe^{II}(CN)_6]_2$ (X = Na, K, Rb or Cs), and representation of the release/intercalation of alkali cations during the redox process.

Having in hands an isostructural series based on either $[Fe^{III}(CN)_6]^{3-}$ or $[Fe^{II}(CN)_6]^{4-}$ anions, the post synthetic chemical reduction of $\mathbf{1}_3$-$[Fe^{III}(CN)_6]_2$ into $K_2\mathbf{1}_3$-$[Fe^{II}(CN)_6]_2$ with hydrazine in partial aqueous solution has already been reported, as shown in figure 1.[40] The reaction follows the equation (1):

$$2\ \mathbf{1}_3\text{-}[Fe^{III}(CN)_6]_{2(s)} + N_2H_{4(aq)} + 4\ K^+ \rightarrow\ 2\ K_2\mathbf{1}_3\text{-}[Fe^{II}(CN)_6]_{2(s)} + 4H^+ + N_{2(g)} \qquad (1)$$

These results were confirmed by X ray diffraction on powder, combined with IR studies. The chemical reduction was followed by a color change of the microcrystalline powder, as shown in figure 1.

Due to the robustness of the $\mathbf{1}_3$-$[Fe^{III}(CN)_6]_2$ and $X_2\mathbf{1}_3$-$[Fe^{II}(CN)_6]_2$ hydrogen bonded networks, the oxidation of $X_2\mathbf{1}_3$-$[Fe^{II}(CN)_6]_2$ (X = Na, K and Cs) was explored. This is a heterogenous oxidation process with oxidizing agents in solution and the hydrogen bonded network in the solid-state. Due to the oxidation potential of $[Fe^{III}(CN)_6]^{3-}/[Fe^{II}(CN)_6]^{4-}$, different oxidizing agents have been tested and the best results have been obtained for peroxodisulfate $S_2O_8^{2-}$.

Chemical oxidation

In this system, the chemical oxidation follows equation (2), $S_2O_8^{2-}$ has been chosen due to its redox potential and its chemical inertness. The reaction is followed by an increase of the concentrations of X^+ and SO_4^{2-} in the solution.

$$X_2\mathbf{1}_3\text{-}[Fe^{II}(CN)_6]_{2(s)} + S_2O_8^{2-}{}_{(aq)} \rightarrow \mathbf{1}_3\text{-}[Fe^{III}(CN)_6]_{2(s)} + 2\ SO_4^{2-}{}_{(aq)} + 2X^+{}_{(aq)} \qquad (2)$$

The microcrystalline powder of $X_2\mathbf{1}_3$-$[Fe^{II}(CN)_6]_2$ (X = Na, K and Cs) was immersed in a solvent mixture (10% Water/90% Methanol) under dynamic condition of exposition to the oxidizing agent (see experimental part), and oxidation was monitored *in situ* by FT-IR at RT for $X_2\mathbf{1}_3$-$[Fe^{II}(CN)_6]_2$ (Na, K and Cs), for a total exposure time of 15000, 16500 and 61200 s respectively. The oxidation

was followed by examining the C≡N stretching band of hexacyanoferrate, expected to occure between 2100 and 1980 cm^{-1}. This band is sensitive to the oxidation state of iron and the symmetry of the ligands.[41,42,43,44] For $K_4Fe^{II}(CN)_6$ and $X_2\mathbf{1}_3$-$[Fe^{II}(CN)_6]_2$, the vibrations are located in the 2060 and 2000 cm^{-1} window, also depending on the deformations encountered by the octahedral environment of Fe(II) (see Table 1). For $K_3Fe^{III}(CN)_6$ and $\mathbf{1}_3$-$[Fe^{III}(CN)_6]_2$ and at room temperature, the ν(C≡N) vibrational modes are located in the 2080 and 2130 cm^{-1} spectral range, as shown by the values provided in table 1. This highest frequency reflects the population decrease of the antibonding highest occupied orbital of the $C\equiv N^-$ ligand.

Compound	ν (C≡N)/ cm^{-1}
$Na_4[Fe^{II}(CN)_6]$	2019, 2048, 2066
$K_4[Fe^{II}(CN)_6]$	2040
$Cs_4[Fe^{II}(CN)_6]$	2040 (2115w)
$K_3[Fe^{III}(CN)_6]$	2118
$\mathbf{1}_3$-$[Fe^{III}(CN)_6]_2$	2108, 2122
$Na_2\mathbf{1}_3$-$[Fe^{II}(CN)_6]_2$	2013, 2031, 2052
$K_2\mathbf{1}_3$-$[Fe^{II}(CN)_6]_2$	2017, 2037, 2054
$Cs_2\mathbf{1}_3$-$[Fe^{II}(CN)_6]_2$	2030, 2049 (2108w, 2122w)

Table 1: Comparison of ν(C≡N)/ cm^{-1} for $\mathbf{1}_3$-$[Fe^{III}(CN)_6]_2$ and $X_2\mathbf{1}_3$-$[Fe^{II}(CN)_6]_2$ (X = Na, K and Cs) and corresponding starting compounds.

Figures 2 a displays the variation of absorbance of ν(C≡N) vibration during the dynamic oxidation process for $Na_2\mathbf{1}_3$-$[Fe^{II}(CN)_6]_2$. For $X_2\mathbf{1}_3$-$[Fe^{II}(CN)_6]_2$ (X = K and Cs), the spectra are presented in figures S3 a and b, in supporting information. For the three compounds, the *in situ* oxidation process was accompanied by a disappearance of the low wavenumber bands and

appearance of bands at high wavenumbers, reflecting the oxidation of $X_2\mathbf{1}_3$-$[Fe^{II}(CN)_6]_2$ (X = Na, K and Cs) into $\mathbf{1}_3$-$[Fe^{III}(CN)_6]_2$.

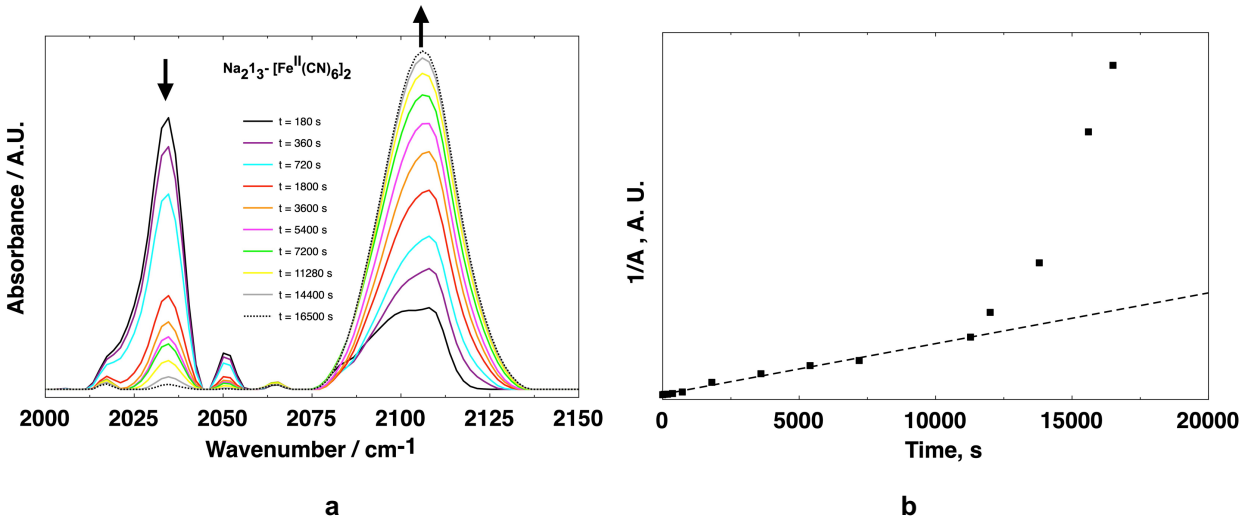

Figure 2: Kinetic study of the oxidation of $Na_2\mathbf{1}_3$-$[Fe^{II}(CN)_6]_2$ into $\mathbf{1}_3$-$[Fe^{III}(CN)_6]_2$ by $S_2O_8^{2-}$ followed at RT by IR spectroscopy in the 2000-2200 cm^{-1} window (a) and plot of 1/A = f(t) where A is the area of the peaks of $Na_2\mathbf{1}_3$-$[Fe^{II}(CN)_6]_2$ located between 2000 and 2060 cm^{-1} (b).

For the three compounds $X_2\mathbf{1}_3$-$[Fe^{II}(CN)_6]_2$ (X = Na, K and Cs), one can note a broadening of the peaks attributed to the appearance of the $[Fe^{III}(CN)_6]^{3-}$ species, presenting a high degree of disorder, as compared to the shape of the corresponding peaks for the freshly prepared $\mathbf{1}_3$-$[Fe^{III}(CN)_6]_2$ (see figure S1, Supporting Information). This is a consequence of the release of X^+ alkali cations during the oxidation process, as shown in figure 1 and equation (2), which causes a disorder in the structure.

In order to estimate the amount of $X_2\mathbf{1}_3$-$[Fe^{II}(CN)_6]_2$ converted into $\mathbf{1}_3$-$[Fe^{III}(CN)_6]_2$, the variation of the area of the peaks attributed to $X_2\mathbf{1}_3$-$[Fe^{II}(CN)_6]_2$ in the 2060-2000 cm^{-1} range was analyzed

as shown in table 2. $Na_2\mathbf{1}_3$-$[Fe^{II}(CN)_6]_2$ exhibits the shortest reaction time with a complete conversion of $Na_2\mathbf{1}_3$-$[Fe^{II}(CN)_6]_2$ into $\mathbf{1}_3$-$[Fe^{III}(CN)_6]_2$.

Compound	$Na_2\mathbf{1}_3$-$[Fe^{II}(CN)_6]_2$	$K_2\mathbf{1}_3$-$[Fe^{II}(CN)_6]_2$	$Cs_2\mathbf{1}_3$-$[Fe^{II}(CN)_6]_2$
Duration of oxidation, s	16500	15000	61200
Amount of oxidized species	100%	75%	50%

Table 2: Amount of oxidized species for the oxidation of $X_2\mathbf{1}_3$-$[Fe^{II}(CN)_6]_2$ (X = Na, K and Cs) into $\mathbf{1}_3$-$[Fe^{III}(CN)_6]_2$ by $S_2O_8^{2-}$ followed at RT by IR spectroscopy for the 2000-2200 cm^{-1} window.

A partial oxidation for $Cs_2\mathbf{1}_3$-$[Fe^{II}(CN)_6]_2$ and $K_2\mathbf{1}_3$-$[Fe^{II}(CN)_6]_2$ is observed (see figures S3 a and b), whereas it is nearly complete for $Na_2\mathbf{1}_3$-$[Fe^{II}(CN)_6]_2$. The IR spectrum of $Cs_2\mathbf{1}_3$-$[Fe^{II}(CN)_6]_2$ is presented in figure S1 (see Supporting Information) and it exhibits a small amount of oxidized species $\mathbf{1}_3$-$[Fe^{III}(CN)_6]_2$, as suggested by the presence of oxidized species in the starting salt $Cs_4[Fe^{II}(CN)_6]$

A preliminarily kinetic study was performed for the oxidation of $Na_2\mathbf{1}_3$-$[Fe^{II}(CN)_6]_2$ into $\mathbf{1}_3$-$[Fe^{III}(CN)_6]_2$. The representation of lnA or 1/A = f(t) (A = area of peaks related to $X_2\mathbf{1}_3$-$[Fe^{II}(CN)_6]_2$ in the 2060 and 2000 cm^{-1} window), was operated and the best results were obtained with the representation of 1/A, as seen in figure 2 b. The kinetics of conversion is coherent, in a first step, with a second order reaction.

The chemical oxidation of $Na_2\mathbf{1}_3$-$[Fe^{II}(CN)_6]_2$ by $S_2O_8^{2-}$ was also followed *in situ* by Raman spectroscopy. The spectra were recorded for a single crystal presenting the following size 5µmx2µmx1µm and under static conditions of exposure to a solvent mixture (10% Water/90% Methanol) containing the oxidizing agent (see experimental section).

There are 3 stretching (C≡N) vibrational modes observed in the Raman spectra of $Na_2\mathbf{1}_3$-$[Fe^{II}(CN)_6]_2$ at 2039 cm^{-1}, 2053 cm^{-1} and 2086 cm^{-1}, and also 3 for $\mathbf{1}_3$-$[Fe^{III}(CN)_6]_2$, observed at 2112 cm^{-1}, 2128 cm^{-1} and 2136 cm^{-1} respectively (figure S4, Supporting Information).[41] During the oxidation process, the decrease of the C≡N vibrational modes of $Na_2\mathbf{1}_3$-$[Fe^{II}(CN)_6]_2$ are observed with a complete disappearance at t = 7200 s, which is shorter than what was observed for the IR study, as shown in figure 3a. This can be explained by the fact that the laser light used in Raman allows to study the oxidation of one micrometric-sized crystal only, whereas in IR the oxidation of a collection of crystals with various sizes is observed.

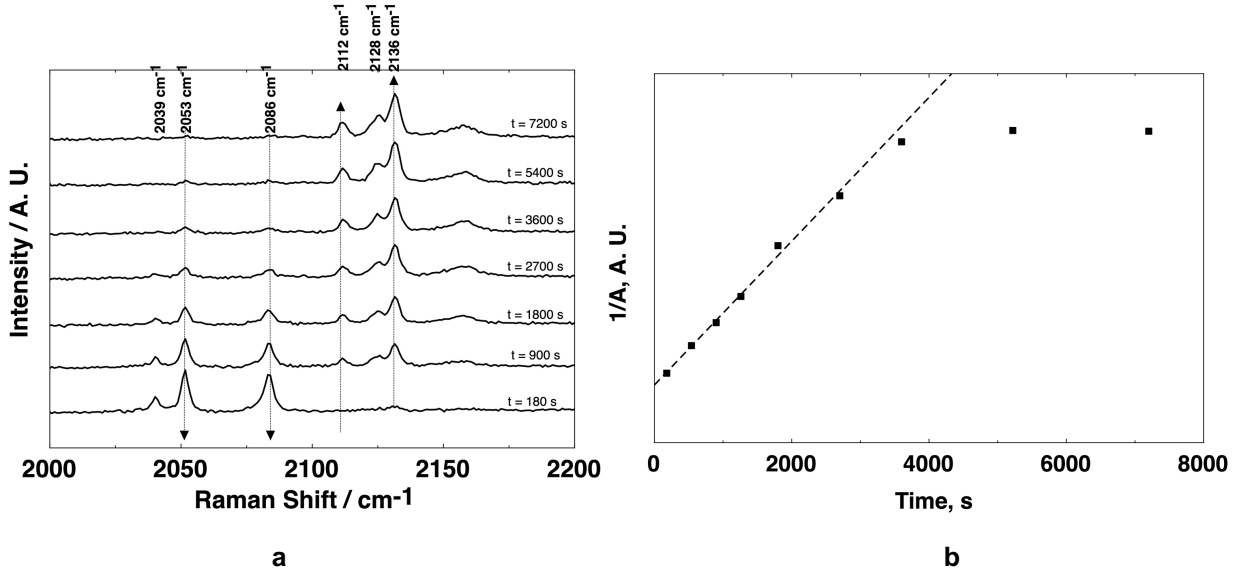

Figure 3: (a) Kinetic study of the oxidation of $Na_2\mathbf{1}_3$-$[Fe^{II}(CN)_6]_2$ into $\mathbf{1}_3$-$[Fe^{III}(CN)_6]_2$ by $S_2O_8^{2-}$ followed at RT by Raman spectroscopy for the 2000-2200 cm^{-1} window and (b) plot of the 1/A =

f(t) where A is the area of the peaks located between 2030 and 2100 cm^{-1}, attributed to $[Fe^{II}(CN)_6]^{4-}$ species.

Similarly to the IR studies, the representation of 1/A = f(t) (A = area of peaks related to $Na_2\mathbf{1}_3$-$[Fe^{II}(CN)_6]_2$ in the 2030 and 2100 cm^{-1} window, as shown in figure 3b shows, in a first step, a linear tendency, which is consistent with a second order reaction for $Na_2\mathbf{1}_3$-$[Fe^{II}(CN)_6]_2$, as also observed by the IR study. The two steps process can be respectively assigned to the oxidation of the surface of the exposed crystal, which is relatively fast, then followed by cascade reactions corresponding to the oxidation of the bulk, which also leads to a release of the Na^+ cations in the solution.

The complete oxidation of $Na_2\mathbf{1}_3$-$[Fe^{II}(CN)_6]_2$ into $\mathbf{1}_3$-$[Fe^{III}(CN)_6]_2$ was also followed by XRPD measurements before and after the oxidation, and the integrity of the hydrogen bonded network was demonstrated after the oxidation process, as shown from the data provided in figure S5 (Supporting Information).

Electrochemical behavior

The oxidation and reduction of the hydrogen bonded network was also investigated by electrochemical means. $[Fe^{III}(CN)_6]^{3-}$ is often used as a model redox mediator in electron transfer processes due to its ideal reversible behavior with anodic and cathodic peak separations (ΔE_p) close to 60 mV, as shown by the CV behavior of a H_2O/MeOH solution of $K_3[Fe^{III}(CN)_6]$ (see figure 4a). The CV curves for a H_2O/MeOH solution of the mixture (**1**-2Cl + $K_3[Fe^{III}(CN)_6]$) displayed a broadening of the $[Fe^{III}(CN)_6]^{3-}$/$[Fe^{II}(CN)_6]^{4-}$ signal after several scans (see figure 4b). ΔE_p increased to 230 mV and the cathodic and cathodic peak currents decreased. No significant

shift of the $[Fe^{III}(CN)_6]^{3-}/[Fe^{II}(CN)_6]^{4-}$ redox potential, however, was observed. After 15 cycles, the electrode was immersed into a fresh H_2O/MeOH solution and the signal persisted suggesting that a probable deposition of the hydrogen bonded network had occurred on the surface as a thin film on the electrode. SEM images of a gold substrate immersed in a solution of (**1**-2Cl + $K_3[Fe^{III}(CN)_6]$) in H_2O/MeOH after 100 Voltammetric cycles (see figure S6 in Supporting Information) confirmed the presence of a deposit on the gold surface. We noted, however, that the deposit looked more amorphous than crystalline, but its morphology and compositions were not further investigated. The incubation time of the gold substrate was either too short to observe the formation of crystals on the gold surface or the application of a potential perturbed their formation.

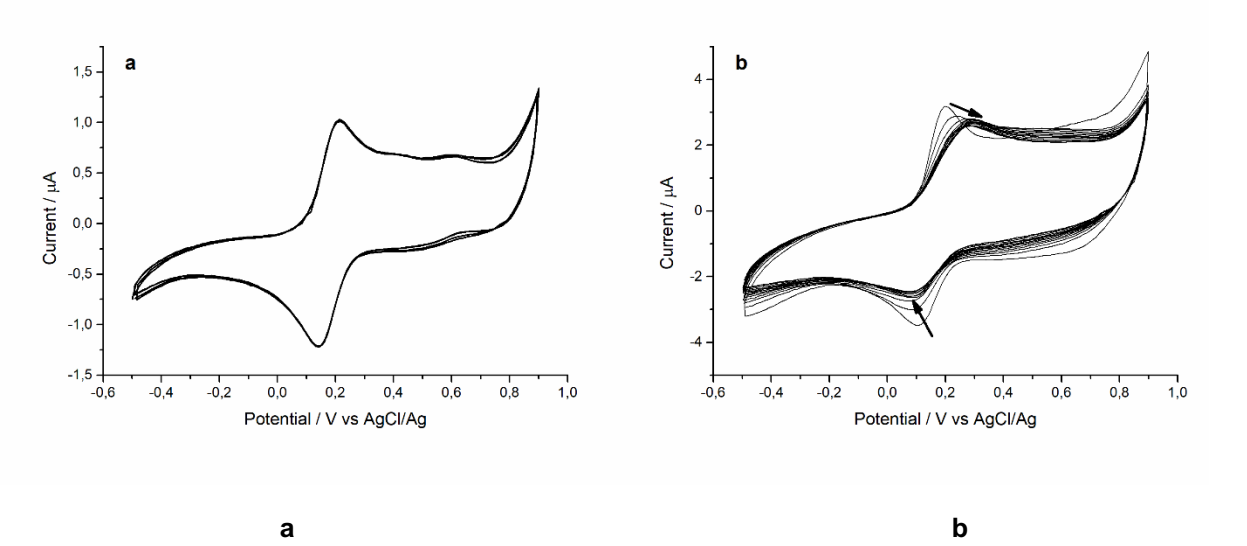

Figure 4: Successive cyclic voltammograms of $K_3[Fe^{III}(CN)_6]$ (a) and (**1**-2Cl + $K_3[Fe^{III}(CN)_6]$) (b) in H_2O/MeOH (9/1) solvent mixture. Scan rate 0.1 $V.s^{-1}$.

Interestingly, after 2h immersion of the gold substrates into either a solution of (**1**-2Cl + $Na_4[Fe^{II}(CN)_6]$) or (**1**-Cl_2 + $K_3[Fe^{III}(CN)_6]$) in H_2O/MeOH, SEM images clearly showed the

presence of microcrystals on the gold surface (figure 5). With $Na_4[Fe^{II}(CN)_6]$) (a), crystals with hexagonal shape can be observed, which is typical of $Na_2\mathbf{1}_3$-$[Fe^{II}(CN)_6]_2$.[39] With the iron(III) salt, the crystals exhibit a different shape, with the presence of holes inside, as already observed for $\mathbf{1}_3$-$[Fe^{III}(CN)_6]_2$.[37] The size of the microcrystals is relatively homogeneous and they both present an hexagonal prismatic shape, with a "diameter" in the range of 2-5 μm.

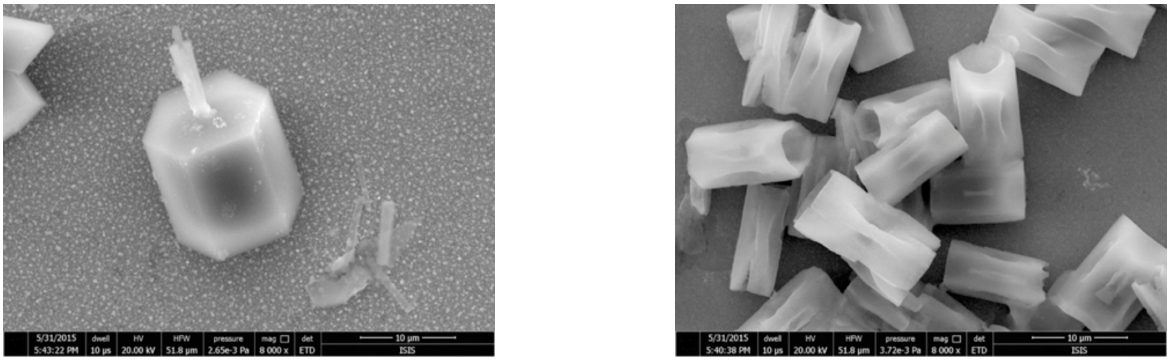

a **b**

Figure 5: SEM SEM micrograph images of $Na_2\mathbf{1}_3$-$[Fe^{II}(CN)_6]_2$ (a) and $\mathbf{1}_3$-$[Fe^{III}(CN)_6]_2$ (b) crystals immobilized at the surface of a gold electrode after immersion process.

The electrochemical behavior of both gold substrates is shown in figure S7 in Supporting Information. Again, the voltammograms reveal large anodic and cathodic signals and a continuous decrease of the signal intensity upon scanning. In both cases, the cathodic signal completely disappears after a few cycles, which suggests that the electrochemical reduction of the H-bonded network is not so easy than its oxidation. The intercalation of the cations (here Na^+) into the crystalline structure upon reduction is thus more difficult than its release during oxidation.

Conclusion

The chemical oxidation, in the solid state, of a molecular hydrogen bonded network, based on dicationic bisamidinium $\mathbf{1}^{2+}$ and $[Fe^{II}(CN)_6]^{4-}$ by $S_2O_8^{2-}$ was evidenced using *in situ* spectroscopic techniques. Depending on the nature of the alkali cation used, different kinetic behaviors were observed. The $Na_2\mathbf{1}_3$-$[Fe^{II}(CN)_6]_2$ network exhibited a complete oxidation within 120 min, in a two-steps process, as shown by FT-IR and Raman spectroscopies. The voltamperometric behavior of ($\mathbf{1}$-Cl_2+ $Na_4[Fe^{II}(CN)_6]$) or ($\mathbf{1}$-Cl_2 + $K_3[Fe^{III}(CN)_6]$) solutions demonstrated the formation of an amorphous compound deposited on the surface of the electrode. These results account for the potential applications of such hydrogen bonded networks as new molecular materials for electrochemical ion intercalation.

ASSOCIATED CONTENT

Supporting Information. Elemental analysis for the used crystalline compounds, FT-IR spectrum of $Cs_2\mathbf{1}_3$-$[Fe^{II}(CN)_6]_2$, Raman spectra of $Na_2\mathbf{1}_3$-$[Fe^{II}(CN)_6]_2$ and $\mathbf{1}_3$-$[Fe^{III}(CN)_6]_2$, XRPD diagram of $Na_2\mathbf{1}_3$-$[Fe^{II}(CN)_6]_2$ after oxidation by $S_2O_8^{2-}$, SEM images of a gold substrate immersed in a solution of ($\mathbf{1}$-2Cl+ $K_3[Fe^{III}(CN)_6]_2$) and cyclic voltammograms of solutions of ($\mathbf{1}$-2Cl+ $Na_2\mathbf{1}_3$-$[Fe^{II}(CN)_6]_2$) and ($\mathbf{1}$-2Cl+ $K_3[Fe^{III}(CN)_6]_2$).

The following files are available free of charge.

AUTHOR INFORMATION

Corresponding Author

ferlay@unistra.fr, hosseini@unistra.fr, hellwig@unistra.fr

Author Contributions

The manuscript was written through contributions of all authors. All authors have given approval to the final version of the manuscript.

ACKNOWLEDGMENT

We thank the Université de Strasbourg, the C.N.R.S., the International centre for Frontier Research in Chemistry (icFRC), the Labex CSC (ANR-10-LABX-0026 CSC) within the Investissement d'Avenir program ANR-10-IDEX-0002-02, the Institut Universitaire de France, the Ministère de l'Enseignement Supérieur et de la Recherche for financial support. Pr. P. Samori and Dr. M. Squillaci are acknowledged for providing SEM images.

REFERENCES

(1) Armand, M.; Tarascon, J.-M. Building Better Batteries. *Nature* **2008**, *451*, 6522-6537.
(2) Dunn, B.; Kamath, H.; Tarascon, J.-M. Electrical Energy Storage for the Grid: A Battery of Choices. *Science* 2011, 334, 928-935.
(3) Special thematic issue on Hybrid Materials. *Chem. Soc. Rev.* **2011**, *40*, 453-1152
(4) Special thematic issue on Metal Organic Frameworks. *Chem. Rev.* **2012**, *112*, 673-1268
(5) Furukawa, H.; Cordova, K. E.; O'Keeffe, M.; Yaghi, O. M. The chemistry and applications of metal-organic frameworks. *Science* **2013**, *341*, 1230444.
(6) R. Taylor and O. Kennard, Hydrogen-bond geometry in organic crystals. *Acc. Chem. Res.*, **1984**, *17*, 320-326.
(7) Desiraju, G. R. *Crystal Engineering: The Design of Organic Solids*; Elsevier: Amsterdam, **1989**.
(8) Etter, M. C. Encoding and decoding hydrogen-bond patterns of organic compounds. *Acc. Chem. Res.,* **1990**, *23*, 120-126.
(9) Hosseini, M. W. Molecular Tectonics: From Simple Tectons to Complex Molecular Networks. *Acc. Chem. Res.* **2005**, *38*, 313-323.
(10) Besenhard J O handbook of battery materials wiley 2008

(11) Ramaswamy P., Wong N.E. Shimizu G.K.H., MOFs as proton conductors - challenges and opportunities. *Chem. Soc. Rev.* **2014**; 43: 5913-5932

(12) Zhao, Y.; Song, Z;. Li, X.; Sun, Q.; Cheng, N.; Lawes, S;. Sun X. Metal organic frameworks for energy storage and conversion. *En. Stor. Mater.* **2016**, 2, 35-62

(13) Wang, H.; Zhu, Q-L.; Zou, R.; Xu Q. Metal-Organic Frameworks for Energy Applications. *Chem*, **2017**, 2, 52-80

(14) Jiang, H.; Liu, X-C.; Wu, Y.; Shu, Y.; Gong, X.; Ke, F-S.; Deng H. Metal-Organic Frameworks for High Charge-Discharge Rates in Lithium-Sulfur Batteries. *Angew. Chem. Int. Ed*, **2018**, *57*, 3916-3921

(15) Indra, A.;, Song, T.; Paik, U. Metal Organic Framework Derived Materials: Progress and Prospects for the Energy Conversion and Storage. *Adv. Mater.* **2018**, *30*, 1705146

(16) Wang, L.; Song, J.; Qiao, R.; Wray, L. A.; Hossain, M. A.; Chuang, Y.-D.; Yang, W.; Lu, Y.; Evans, D.; Lee, J.-J.; Vail, S.; Zhao, X.; Nishijima, M.; Kakimoto, S.; Goodenough, J. B. Rhombohedral Prussian White as Cathode for Rechargeable Sodium-Ion Batteries. *J. Am. Chem. Soc.* **2015**, 137, 2548-2554.

(17) Nie, P.; Shen, L.; Luo, H.; Ding, B.; Xu, G.; Wang, J.; Zhang, X. Prussian Blue Analogues: a New Class of Anode Materials for Lithium Ion Batteries. *J. Mater. Chem. A* **2014**, *2*, 5852-5857.

(18) Hurlbutt, K.; Wheeler, S.; Capone, I.; Pasta M. Prussian Blue Analogs as Battery Materials. *Joule*, **2018**, doi.org/10.1016/j.joule.2018.07.017

(19) Ling, C.; Chen, J.; Mizuno F. First-Principles Study of Alkali and Alkaline Earth Ion Intercalation in Iron Hexacyanoferrate: The Important Role of Ionic Radius. *J. Phys. Chem. C* **2013**, 117, 21158-21165

(20) Watanabe, M.; Thomas, M. L.; Zhang, S.; Ueno, K.; Yasuda, T;. Dokko K. Application of Ionic Liquids to Energy Storage and Conversion Materials and Devices. *Chem. Rev.*, **2017**, 117, 10, 7190-7239

(21) Page, K. A.; Rowe, B. W. An Overview of Polymer Electrolyte Membranes for Fuel Cell Applications, 2012, Polymers for Energy Storage and Delivery: Polyelectrolytes for Batteries and Fuel Cells Chapter 9, pp 147-164 *ACS*

(22) Shimizu, G. K. H.; Taylor, J. M.; Kim S-R. Proton Conduction with Metal-Organic Frameworks. *Science*, **2013**, *341*, 354-355

(23) Schröder, U.; Scholz F. The Solid-State Electrochemistry of Metal Octacyanomolybdates, Octacyanotungstates, and Hexacyanoferrates Explained on the Basis of Dissolution and Reprecipitation Reactions, Lattice Structures, and Crystallinities. *Inorg. Chem.* **2000**, *39*, 1006-1015

(24) Mizuno, Y.; Okubo, M.; Kagesawa, K.; Asakura, D.; Kudo, T.; Zhou, H.; Ohishi, K.; Okazawa, A.; Kojima N. Precise Electrochemical Control of Ferromagnetism in a Cyanide-Bridged Bimetallic Coordination Polymer. *Inorg. Chem.* **2012**, *51*, 10311-10316

(25) Long, J.; Asakura, D.; Okubo, M.; Yamada, A.; Guari, Y.; Larionova J. Electrochemical Li-Ion Intercalation in Octacyanotungstate-Bridged Coordination Polymer with Evidence of Three Magnetic Regimes. *Inorg. Chem.* **2016**, *55*, 7637-7646

(26) Okubo, M.; Kagesawa, K.; Mizuno, Y.; Asakura, D.; Hosono, E.; Kudo, T.; Zhou, H.; Fujii, K.; Uekusa, H.; Nishimura, S.-i.; Yamada, A.; Okazawa, A.; Kojima, N. Reversible Solid State Redox of an Octacyanometallate-Bridged Coordination Polymer by Electrochemical Ion Insertion/Extraction. *Inorg. Chem.* **2013**, *52*, 3772-3779.

(27) Nafady, A.; Bond, A. M.; Bilyk A. Controllable Synthesis and Fabrication of Semiconducting Nanorod/Nanowire Bundles of $Fe[TCNQ]_2(H_2O)_2$ via Electrochemically Induced

Solid-Solid Phase Transformation of TCNQ Microcrystals. *J. Phys. Chem. C* **2008**, *112*, 6700-6709

(28) Ward, M. D.Design of crystalline molecular networks with charge-assisted hydrogen bonds. *Chem. Commun.,* **2005**, 5838.

(29) Holman, K. T.; Pivovar, A. M.; Ward M. D. Engineering Crystal Symmetry and Polar Order in Molecular Host Frameworks. *Science*, **2001**, *294*, 1907-1911.

(30) Saied, O., Maris, T., Wuest, J. D. Deformation of Porous Molecular Networks Induced by the Exchange of Guests in Single Crystals. *J. Am. Chem. Soc*. **2003**, *125*, 14956-14957.

(31) Chen, C.-L.; Beatty, A. M. Guest Inclusion and Structural Dynamics in 2-D Hydrogen-Bonded Metal-Organic Frameworks. *J. Am. Chem. Soc*., **2008**, *130*, 17222-17223.

(32) Shimizu, G. K. H., Vaidhyanathan, R.; Taylor, J. M. Phosphonate and sulfonate metal organic frameworks. *Chem. Soc. Rev*. **2009**, *38*, 1430-1449.

(33) Hosseini, M. W. Molecular tectonics: from molecular recognition of anions to molecular networks. *Coord. Chem. Re*v. **2003**, *240*, 157-166.

(34) Cvrtila, I.; Stilinović, V. New Tricks by Old Anions: Hydrogen Bonded Hexacyanoferrous Anionic Networks. *Cryst. Growth Des*. **2017**, *17*, 6793-6800.

(35) Ferlay, S; Hosseini, M. W. Molecular Tectonics: Design of Hybrid Networks and Crystals based on Charge-Assisted Hydrogen Bonds. In Eds. P. Samorì and F. Cacialli, Wiley-VCH, **2011**.

(36) Ferlay, S. ; Félix, O. ; Hosseini, M. W. ; Planeix, J.-M. ; Kyritsakas, N. Second sphere supramolecular chirality: racemic hybrid H-bonded 2-D molecular networks. *Chem. Commun.,* **2002**, 702-703.

(37) Ferlay, S.; Bulach, V.; Felix, O.; Hosseini, M. W.; Planeix, J.-M.; Kyritsakas, N. Molecular tectonics and supramolecular chirality: rational design of hybrid 1-D and 2-D H-bonded molecular networks based on bis-amidinium dication and metal cyanide anions. *CrystEngComm*, **2002**, *4*, 447-453.

(38) Dechambenoit, P.; Ferlay, S.; Hosseini, M. W.; Planeix, J.-M.; Kyritsakas Molecular tectonics: control of packing of hybrid 1-D and 2-D H-bonded molecular networks formed between bisamidinium dication and cyanometallate anions. *New. J. Chem.,* **2006**, *30*, 1403-1410.

(39) Dechambenoit, P.; Ferlay, S.; Kyritsakas N.; Hosseini M. W. Molecular tectonics: crystal engineering of mixed valence Fe(II)/Fe(III) solid solutions. *Chem. Commun*., **2010**, 868-870.

(40) Dechambenoit, P.; Ferlay, S.; Kyritsakas, N.; Hosseini M. W. *In situ* reduction of Fe(III) into Fe(II): an example of post-crystallisation transformation. *Chem. Commun.,* **2009**, 6798-6800

(41) Nakamoto, K. *Infrared and Raman Spectra of Inorganic and Coordination Compounds,* Wiley, New York, **1963**.

(42) Nath Gosh, S. Infrared spectra of the Prussian blue analogs. *J. Inorg. Nucl. Chem.,* **1974**, *36*, 2465-2466.

(43) Dobson, K.; Mc Quillan, A. J. An *in situ* IR spectroscopic investigation of adsorption of hexa- and penta-cyanoferrates to metal oxides from aqueous solution. *Phys. Chem. Chem. Phys.,* **2000**, *2*, 5180-5188.

(44) Ferlay, S.; Hellwig, P.; Hosseini, M. W. Partially Reversible Thermal-Induced Oxidation During a Dehydration Process in an H-bonded Supramolecular System. *ChemPhysChem*, **2018**, doi:10.1002/cphc.201800845.

SYNOPSIS

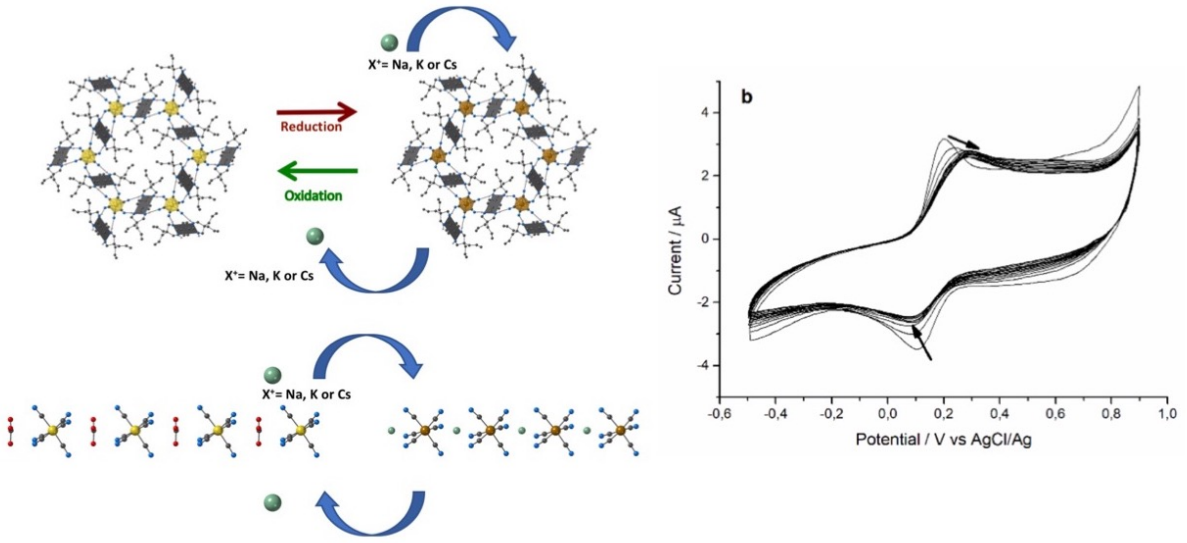
X⁺= Na, K or Cs
Reduction
Oxidation
X⁺= Na, K or Cs
X⁺= Na, K or Cs
b
Current / µA
Potential / V vs AgCl/Ag